Article

Cell

Prefrontal Parvalbumin Neurons in Control of Attention

Graphical Abstract

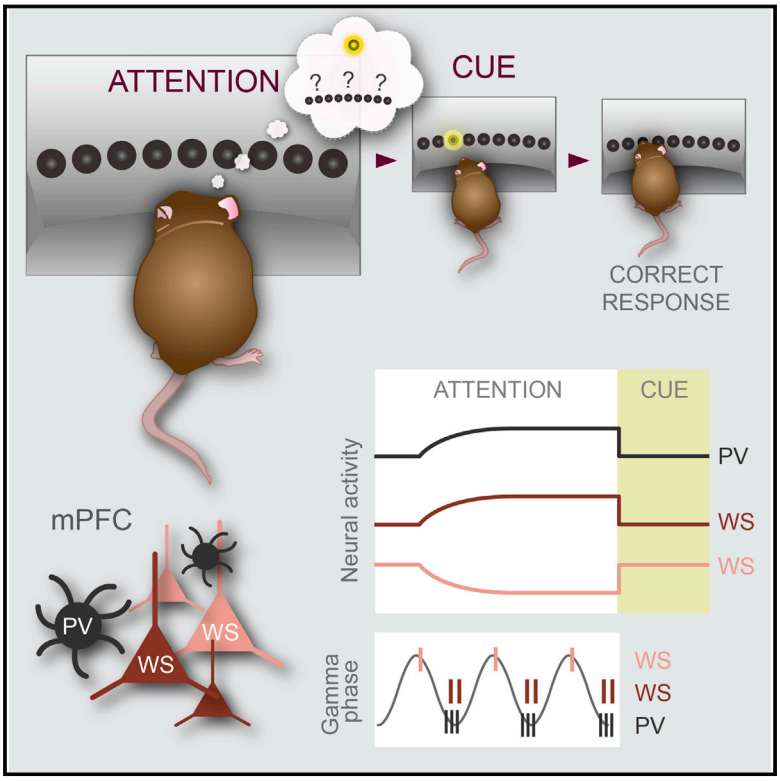

Authors

Hoseok Kim, Sofie Ährlund-Richter, Xinming Wang, Karl Deisseroth, Marie Carlén

Correspondence

marie.carlen@ki.se

In Brief

A combination of electrophysiology and optogenetic manipulations reveal that inhibitory parvalbumin interneurons and gamma oscillations are central to prefrontal cortex's control of attention.

Highlights

- Increased firing of mPFC PV interneurons is a signature of top-down attention
- Attention is characterized by synchronization of mPFC PV neurons and elevated gamma
- Local pyramidal neurons show gamma-phase-dependent rate modulation during attention
- Synchronization of mPFC PV neurons at gamma frequencies has pro-cognitive effects

Kim et al., 2016, Cell *164*, 208–218
January 14, 2016
http://dx.doi.org/10.1016/j.cell.2015.11.038

CellPress

Cell

Article

Prefrontal Parvalbumin Neurons in Control of Attention

Hoseok Kim,[1] Sofie Ährlund-Richter,[1] Xinming Wang,[1] Karl Deisseroth,[2,3,4] and Marie Carlén[1,*]
[1]Department of Neuroscience, Karolinska Institutet, Retzius väg 8, 171 77 Stockholm, Sweden
[2]Howard Hughes Medical Institute
[3]Department of Bioengineering
[4]Department of Psychiatry and Behavioral Sciences
W080 Clark Center, 318 Campus Drive West, Stanford University, Stanford, CA 94305, USA
*Correspondence: marie.carlen@ki.se
http://dx.doi.org/10.1016/j.cell.2015.11.038

SUMMARY

While signatures of attention have been extensively studied in sensory systems, the neural sources and computations responsible for top-down control of attention are largely unknown. Using chronic recordings in mice, we found that fast-spiking parvalbumin (FS-PV) interneurons in medial prefrontal cortex (mPFC) uniformly show increased and sustained firing during goal-driven attentional processing, correlating to the level of attention. Elevated activity of FS-PV neurons on the timescale of seconds predicted successful execution of behavior. Successful allocation of attention was characterized by strong synchronization of FS-PV neurons, increased gamma oscillations, and phase locking of pyramidal firing. Phase-locked pyramidal neurons showed gamma-phase-dependent rate modulation during successful attentional processing. Optogenetic silencing of FS-PV neurons deteriorated attentional processing, while optogenetic synchronization of FS-PV neurons at gamma frequencies had pro-cognitive effects and improved goal-directed behavior. FS-PV neurons thus act as a functional unit coordinating the activity in the local mPFC circuit during goal-driven attentional processing.

INTRODUCTION

Attention plays a crucial role in our ability to organize thoughts and actions in meaningful behavior. On a neurophysiological level, attention biases processing of certain neural representations at the expense of others. As a result, behaviorally relevant information is amplified, while distracting or irrelevant information is suppressed (Noudoost et al., 2010). The prefrontal cortex (PFC) directly influences attentional processing (Baluch and Itti, 2011; Clark et al., 2015; Gregoriou et al., 2014; Miller and Buschman, 2013; Moore and Armstrong, 2003; Zhang et al., 2014), but the local computations underlying PFC's control of attention have not been established. Cortical inhibitory interneurons expressing parvalbumin (PV) are powerful regulators of local network activities (Hu et al., 2014), and synchronous activation of PV neurons is sufficient for induction of gamma oscillations (30–80 Hz) (Buzsáki and Wang, 2012; Cardin et al., 2009; Sohal et al., 2009). PV neurons in sensory areas contribute to the signatures of attention through local modulation of sensory responses (Atallah et al., 2012; Lee et al., 2012; Wilson et al., 2012), including through the expression of gamma oscillations (Siegle et al., 2014). Importantly, attentional processing is characterized by increases in gamma activity, both in sensory as well as prefrontal areas (Gregoriou et al., 2014) (Gregoriou et al., 2015).

Activity of cortical PV neurons is not only essential for microcircuit operations but does also correlates to behavioral events (Isomura et al., 2009; Kvitsiani et al., 2013), and recent findings suggest that prefrontal PV neurons can act as a functional unit able to orchestrate the flow of information in and between brain areas (Courtin et al., 2014; Kepecs and Fishell, 2014). Given the functional repertoire of PV neurons, it is not surprising that this neuronal cell type repetitively has been implicated in a variety of neurological and psychiatric diseases (Marín, 2012). The links are especially strong in schizophrenia, a disabling mental disorder with well-defined impairments in the control of attention (Lustig et al., 2013). Patients with schizophrenia demonstrate impairment in visual search when top-down goals are required, showing a selective deficit in top-down control of attention (Gold et al., 2007). Cognitive deficits in schizophrenia are suggested to emerge from impaired prefrontal gamma oscillations (Lewis et al., 2012), and the key role of PV neurons in the generation of cortical gamma oscillations links this neuronal class to cognitive deficits (Carlén et al., 2012; Korotkova et al., 2010).

Despite many intersecting lines of circumstantial evidence, proof for a function of inhibitory medial PFC (mPFC) PV neurons in the control of attention is lacking. Moreover, it is yet to be demonstrated how cortical PV neurons relate to gamma activity in attention and how prefrontal gamma oscillations could contribute to the behavioral benefits of attention. Elucidation of the circuit underpinnings of top-down control of attention will not only give answers to central questions regarding how PFC contributes to purposeful behavior, but will also give insight on how circuit disturbances could underlie symptomatology in mental disorders characterized by altered cognition.

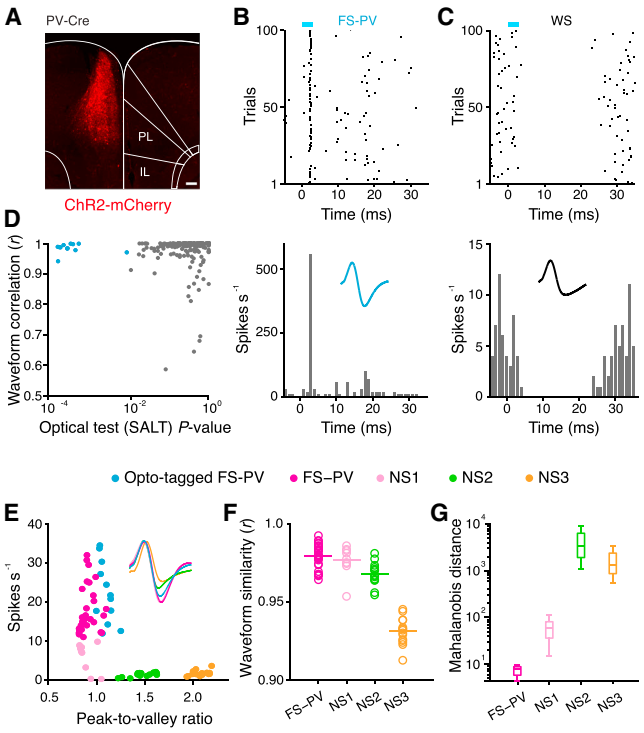

Figure 1. Optogenetic Tagging and Classification of mPFC FS-PV Neurons in Freely Moving Mice

(A) Expression of ChR2-mCherry (red) in mPFC FS-PV neurons in a PV-Cre mouse injected unilaterally with AAV DIO ChR2-mCherry. (n = 4 PV-Cre mice). PL, prelimbic; IL, infralimbic. Scale bar, 100 μm.

(B and C) Raster plot (top) and peri-stimulus time histogram (PSTH; bottom) of a light-activated FS-PV neuron (B) and an inhibited WS neuron recorded from the same tetrode (C), both aligned to light onset. Insets display representative spike waveforms.

(D) Scatter plot of SALT versus waveform correlation for identification of directly light-activated neurons (n = 252 analyzed neurons). Optically tagged neurons (n = 12, $p < 0.01$ by SALT; blue) display high waveform correlation between light evoked and spontaneous spikes ($r > 0.9$).

(E) Scatter plot of firing rate versus peak-to-valley ratio for opto-tagged FS-PV units and all recorded NS units. Opto-tagged FS-PV units (blue) cluster with FS-PV neurons identified by electrophysiological properties (purple). Inset displays representative spike waveforms.

(F) Waveform similarity between opto-tagged FS-PV and recorded NS neurons. $r = 1.0$: a waveform identical to the waveform of opto-tagged FS-PV neurons.

(G) Mahalanobis distance between the cluster of opto-tagged FS-PV neurons and clusters of recorded NS neurons.

See also Figure S2.

RESULTS

Identification and Recording of mPFC Neurons during Top-Down Control of Attention

To characterize the recruitment and firing modulation of mPFC neurons during attentional processing, we conducted chronic electrophysiological recordings in mice performing a three-choice version of the five-choice serial reaction time task (5-CSRTT) (Robbins, 2002). The 5-CSRTT is a widely employed rodent attention task, building on tests of sustained attention originally developed for humans, and is identified as having high construct validity (Lustig et al., 2013). In the task, animals are required to orient to an array of stimulus presentation holes in an operant chamber and to allocate attention to detect and report the location of a brief visual stimulus (cue) presented pseudorandomly in one of three presentation holes (Figure S1A and Movie S1). The animals were subjected to a six-step training schedule defined by specific criteria (modified from Bari et al. [2008]) (Figures S1B–S1F) to fully learn the task (n = 28 ± 8 training days for all animals used, n = 13 PV-Cre mice). After meeting the target criteria, three PV-Cre mice were implanted with microdrives holding four movable tetrodes targeted to prelimbic (PL) and infralimbic (IL) cortex (Figures S2A–S2C), and 426 well-isolated neurons were recorded during 3-CSRTT (54 sessions, 3,857 trials in total). As a first step, we classified the recorded units into narrow-spiking (NS; n = 70, half-valley width 252 ± 36 μs) putative inhibitory interneurons and wide-spiking (WS; n = 329, half-valley width 428 ± 37 μs) putative pyramidal neurons based on spike waveform features (Stark et al., 2013; Figure S2D). Units with low classification confidence ($p > 0.05$, n = 27) were not classified. The waveform classification revealed three potential NS clusters, and the units were therefore further classified based on firing rate (Figure S2E). This parameter identified a population of fast-spiking NS neurons, and NS units with an average firing rate > 10 Hz were classified as FS-PV neurons (n = 30, mean firing rate 18 ± 6 Hz, all data from all trials). Inhibitory interactions and short-latency suppression of WS spiking were confirmed for 21 of the 30 FS-PV neurons in computed cross-correlograms (Fujisawa et al., 2008; see further below).

Optogenetics enables verification of physiology-based classification of neurons recorded in vivo (Kvitsiani et al., 2013; Roux et al., 2014), and we therefore paired chronic extracellular recordings with optical tagging of FS-PV neurons in freely moving animals (n = 4 PV-Cre mice, 46 opto-tagging sessions). An adeno-associated virus expressing channelrhodopsin-2 (ChR2) (Cardin et al., 2009) was targeted to mPFC to render PV neurons sensitive to blue light (Figure 1A). Application of blue light (473 nm, 5 mW, 3–5 ms light pulses, 10–90 Hz) elicited short-latency action potentials in ChR2-expressing FS-PV neurons followed by inhibition of WS neurons recorded on the same tetrode (Figures 1B and 1C), demonstrating efficient temporal control of FS-PV neuron activity during active behavior. Using stimulus-associated spike latency test (SALT) in combination with a spike-shape correlation measure (Kvitsiani et al., 2013), we confirmed that the 12 units optically tagged and recorded were directly light-driven FS-PV neurons (Figure 1D). Comparison of the electrophysiological properties between NS neurons recorded during 3-CSRTT and FS-PV neurons identified through opto-tagging confirmed that our physiological classification correctly categorized FS-PV neurons (Figures 1E–1G).

FS-PV Neurons, but Not WS Neurons, Closely Track Attention

The 3-CSRTT assesses attentiveness to multiple locations and the speed of processing over a large number or trials. Incorrect reporting of stimulus location (nose-poke response into wrong hole; Movie S3), premature reporting (nose-poke response before cue onset; Movie S2), and omission (failure to report

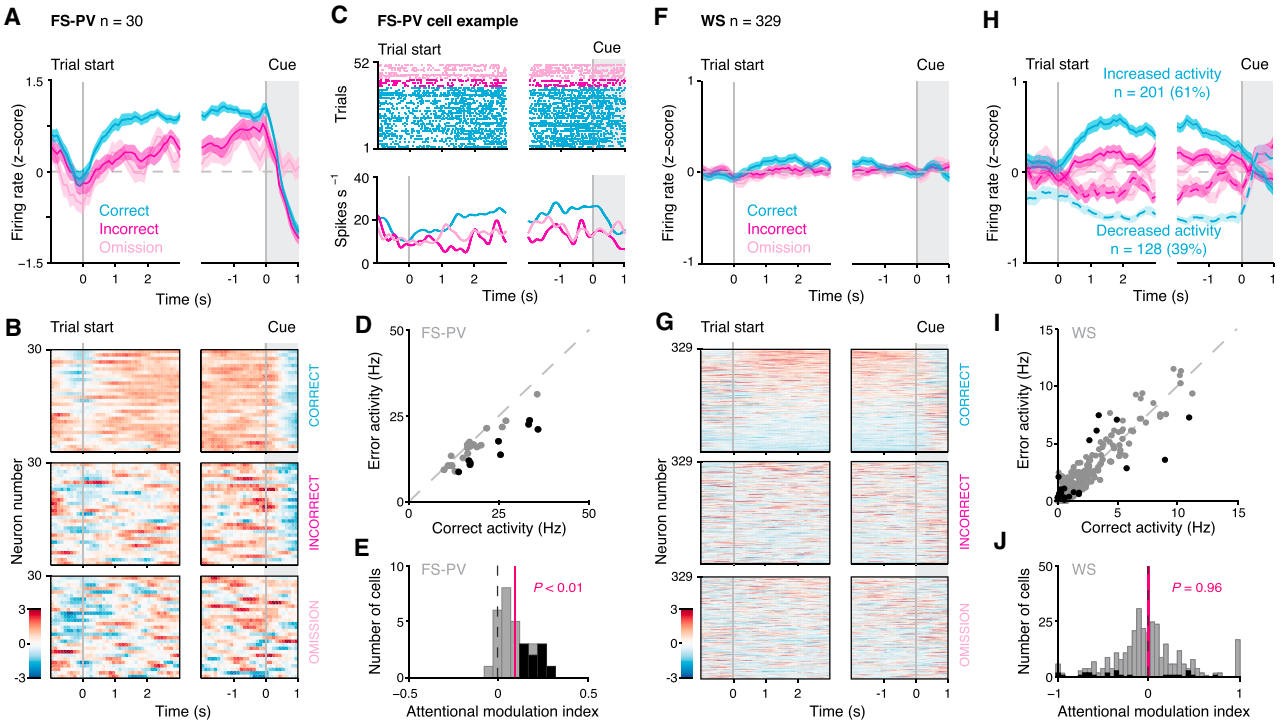

Figure 2. Firing Modulation of mPFC FS-PV and WS Neurons during Attentional Processing

(A–C) and (F–H) PETH aligned to trial start and to cue onset for all FS-PV (n = 30) and WS neurons (n = 329) recorded in the 3-CSRTT. The timeline is broken due to the pseudorandom delay. 500 ms sliding window, 100 ms time bins.

(A) Mean *Z* scores of responses of the whole FS-PV population based on the behavioral outcome of the trials (correct, blue; incorrect, purple; omission, pink). Shaded areas, SEM.

(B) Individual mean *Z* scores of all recorded FS-PV neurons. The neurons are plotted in the same order for the three behavioral outcomes with the colors indicating low (blue) to high (red) firing rate.

(C) Spike raster (top) and spike density functions (a guassian kernel σ = 100 ms; bottom) of an example FS-PV neuron based on the behavioral outcome of each trial; colors as in (A).

(D) Comparison of the average firing rate of the recorded FS-PV neurons in correct versus error (incorrect + omission) trials, 1 s (−1 to 0 s) before cue onset. 9 out of 30 FS-PV neurons display a significantly increased firing rate in correct trials (black dots; $p < 0.05$, Wilcoxon rank-sum test).

(E) Attentional modulation index of the FS-PV population (red line; 0.1 ± 0.09, mean ± SD; $p < 0.01$, t test). 30% of the individual neurons are significantly modulated by attention (black; $p < 0.05$, Wilcoxon rank-sum test). Positive values refer to enhanced spiking in correct trials, and negative values refer to enhanced spiking in error trials.

(F) Mean *Z* scores of responses of the whole WS population based on the behavioral outcome of the trials. Colors as in (A); shaded areas, SEM.

(G) Individual mean *Z* scores of all recorded WS neurons. The neurons are plotted in the same order for the three behavioral outcomes with the colors indicating low (blue) to high (red) firing rate.

(H) Mean *Z* scores of responses of all WS neurons based on behavioral outcome and on whether a neuron displays a mean increased or decreased activity during the delay of correct trials (blue). This dissociates the neurons into one population with increased activity (solid line) and one population with decreased activity (dashed line). The two populations display less dissociated activities during incorrect (purple) and omitted (pink) trials. Shaded areas, SEM.

(I) Comparison of the average firing rate of the recorded WS neurons in correct versus error (incorrect + omission) trials 1 s (−1 to 0 s) before cue onset. 9 out of 329 neurons (2.7%) show significantly increased activity in correct trials and 16 out of 329 neurons (4.9%) in error trials (black dots; $p < 0.05$, Wilcoxon rank-sum test).

(J) Attentional modulation index of the WS population (red line; 0.0 ± 0.4, mean ± SD; $p = 0.96$, t test). Colors as in (E).

See also Figures S1 and S3.

cue location within a defined time span; Movie S4) are scored as errors and are considered to reflect disturbances in attentional processing and executive functioning (Robbins, 2002). To increase the attentional load and prevent self-pacing strategies for prediction of stimulus onset, we employed pseudorandom delays ("delay" refers to time from trial start to cue onset) with the cue being presented 3, 4, or 5 s after trial start, on a trial-to-trial basis ("event onset asynchrony").

We focused our examination of the responses of the recorded FS-PV and WS populations to the delay (i.e., when attention is allocated [Totah et al., 2009, 2013; Figure S1A]). The firing rate modulation was analyzed based on the behavioral outcome (correct, incorrect, or omitted response). Premature responses cancel cue presentation, and we therefore did not perform analysis of recordings from trials with this type of error. Trial start was reported by an increase in FS-PV activity, independent of behavioral outcome (Figure 2A). However, in trials with correct report of cue location, the FS-PV neurons uniformly displayed a sustained enhancement of firing during the delay compared to trials with incorrect report or omission (Figures 2A–2D). Already 300 ms

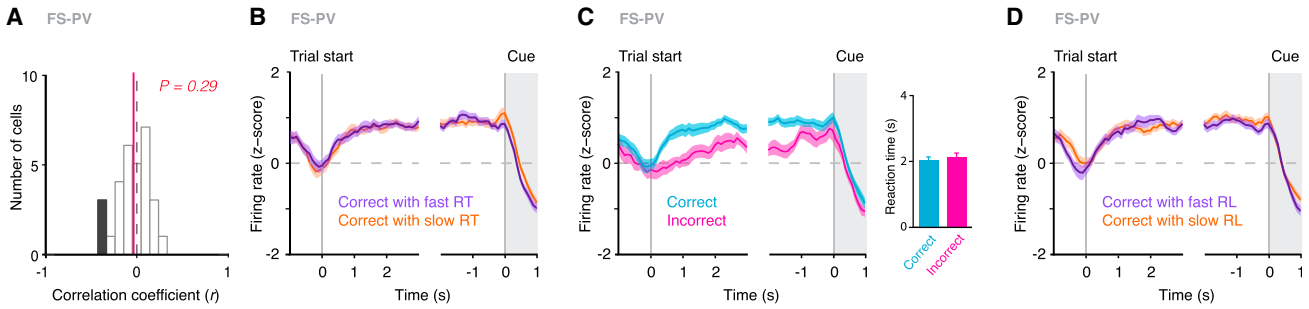

Figure 3. The mPFC FS-PV Activity Correlates to Attentional Processing

(A–D) FS-PV neurons, n = 30.

(A) There is no correlation between the FS-PV activity (−1 to 0 s before cue onset) and the reaction time (RT) in correct trials (red line; $r = 0.04 \pm 0.19$, mean ± SD; p = 0.29, t test). Black indicates significance ($p < 0.05$).

(B) FS-PV activity during attentional processing in correct trials based on the RT (slow or fast).

(C) FS-PV activity during attentional processing for correct and incorrect trials with similar RT.

(D) FS-PV activity during attentional processing in correct trials based on the latency to collect reward (RL; slow or fast).

Shaded areas, SEM. See also Figure S4.

after trial start, the FS-PV activity was significantly higher in correct trials compared to error trials (incorrect + omission). It was thus possible, based on the level of the FS-PV activity, to predict successful behavior (i.e., correct response) more than 2.5 s before cue onset ($p < 0.05$, paired t test, example from shortest delay [3 s]). As a population, the FS-PV neurons showed a remarkably homogenous firing rate modulation during the delay preceding a successful behavioral response (Figure 2B), with up to 40% of the neurons displaying significantly elevated firing rates in correct trials (Figure S3A). As a whole, the FS-PV activity was modulated by attention (Figure 2E).

Analysis of the firing rate of the WS population (n = 329) revealed only minor modulations throughout the delay, regardless of behavioral outcome (Figure 2F). Yet, the elevated FS-PV firing is expected to exert pronounced inhibitory effects on local WS spiking (Hu et al., 2014; Roux and Buzsáki, 2015). In support of this, we found a high prevalence of short-latency inhibitory putative monosynaptic interactions between FS and WS neurons in computed cross-correlograms (Fujisawa et al., 2008), identifying functional connectivity between the cell types and FS-PV suppression of WS spiking (Figure S3B). We therefore next analyzed the firing rate modulation during the delay of correct trials for each WS neuron individually (Figures 2G and S3C). Interestingly, this revealed a clear dissociation of the WS population, with 61% of the WS neurons showing elevated activity and 39% suppressed activity (Figures 2G and 2H). Mixed modulation of mPFC activity during attentional processing has been observed in the 3- and 5-CSRTT in earlier studies, in which the recorded neurons were not classified into cell types (Donnelly et al., 2015; Totah et al., 2009). Importantly, the WS sub-population with enhanced activity in correct trials displayed lower firing rates in error trials (Gregoriou et al., 2014; Figure 2H). Conversely, the WS subpopulation with suppressed activity in correct trials was less suppressed in error trials (Figure 2H). In line with this, the strongest and fastest inhibition by FS-PV neurons was seen in correct trials, targeting the WS sub-population with suppressed activity (trough at 3 ms in correct trials and 4 ms in error trials for WS neurons with suppressed activity; Figure S3D). Taken together, WS neurons showed mixed activities during attentional processing (Figures 2I and S3E), but the WS activity as a whole was not modulated by attention (Figure 2J).

The response latency (i.e., the reaction time: time from cue onset to nose-poke response) correlated to trial outcome, corroborating previous findings (Totah et al., 2009), with faster responses in correct trials compared to incorrect trials (correct: 1.7 ± 0.3 s; incorrect: 2.1 ± 0.5 s, $p < 0.01$, paired t test), even during training (Figure S1F). Interestingly, there was no correlation between the reaction time and the FS-PV activity directly before cue onset in correct trials (i.e., the time point when the animals most urgently must allocate attention in order to not miss the presentation of the cue [Figure 3A]). Further, the pattern of FS-PV activity was indistinguishable between correct trials with fast and slow reaction times (Figure 3B). These findings suggest that the recorded FS-PV activity does not correlate to general task engagement (Hayden et al., 2009) or motor preparation. In support of this, the FS-PV activity was modulated differently in correct and incorrect trials with very similar reaction times (i.e., although the behavioral responses were performed with very similar latencies, the FS-PV activity clearly reflected the respective trial type's level of attention and predicted the outcome of the behavior [Figure 3C]).

Analysis of the latency to collect reward after correct responses (reward collection latency, RL; Figure S1A) provides a sensitive control measure of motivation, with longer reward latencies reflecting lowered motivation (Robbins, 2002). We found that the FS-PV activity during attentional processing in correct trails with fast reward latencies was not different from the activity in correct trials with slow reward latencies, arguing against the recorded FS-PV activity being a correlate of the motivational state of the animal (Figure 3D). Collectively, these findings lend support to the interpretation that elevated and sustained mPFC FS-PV delay activity is a correlate of successful attentional processing.

Error or reward processing could potentially influence the neuronal activity in a subsequent trial, and we therefore investigated how the FS-PV activity during the delay was affected by

the outcome of previous behavior (i.e., if the previous trial was rewarded or not). The level of FS-PV activity during the delay of trials with correct responses was very similar, regardless of whether the previous trial was rewarded or not, with the distinction that the elevation of activity came significantly earlier if the previous trial had been rewarded ($p < 0.01$, paired t test; Figure S4). This suggests that the consequence of the animal's previous behavior does not affect the level of recruitment of mPFC FS-PV neurons but possibly influences the timing of recruitment.

Successful Allocation of Attention Is Characterized by Synchronization of mPFC FS-PV and WS Neurons and Enhanced Gamma Oscillations

Allocation of attention is correlated to enhancement of gamma synchronization in PFC (Gregoriou et al., 2009, 2015), and it has been proposed that oscillations in the gamma range benefit cortical processing and behavior (Fries, 2009; Pritchett et al., 2015). Analysis of the local field potential (LFP) revealed distinct bouts of spontaneously occurring gamma during the delay in trials with correct responses (Figure 4A). The 30–40 Hz gamma activity was significantly elevated in correct trials compared to trials with omitted responses. Trials with incorrect report of cue location showed intermediate levels of gamma activity, possibly reflecting the notion that attention is indeed engaged in incorrect trials, but not sufficiently to support correct report of the cue location (Totah et al., 2009; Figures 4B–4D). Importantly, the gamma amplitude did not differ between trial types directly after termination of the delay (i.e., the elevation of gamma in correct trials was specific to the time point when attention was allocated [Figures 4D and 4E]).

Optogenetics has provided causative in vivo evidence for the crucial role of FS-PV neurons in the emergence of cortical gamma oscillations; ChR2 drive of FS-PV neurons at gamma frequencies entrain naturalistic gamma in the local in vivo circuit (Cardin et al., 2009; Siegle et al., 2014; Sohal et al., 2009). To infer whether gamma activity coupled to attention depends on synchronous firing of mPFC FS-PV neurons, we investigated the alignment and level of phase locking of FS-PV firing during the last 2 seconds of the delay. The FS-PV population was significantly phase locked (Vinck et al., 2013) and fired in the same phase (the trough) of the gamma cycle in all types of trials, with strongest phase locking in correct trials (i.e., during successful allocation of attention characterized by elevated gamma activity [Figure 4F]). Selective investigation of significantly phase-locked FS-PV neurons revealed a strong phase concentration of the spiking in the trough of the gamma cycle (Siegle et al., 2014) in correct trials (Figure 4G). This pronounced synchronous FS-PV firing was followed by a period of suppressed local WS firing (Figures 4H and 4I). Further, in correct trials, the WS firing became significantly phase locked to gamma (Figures 4H and 4I). This characteristic pattern and alignment of FS-PV phase-locking are consistent with the dynamics of FS-PV-driven gamma (Pritchett et al., 2015 but see Buzsáki and Wang, 2012). Taken together, successful allocation of attention was characterized by gamma-rhythmic inhibition by FS-PV neurons, increased temporal precision of WS firing, and synchronization of WS firing (Hasenstaub et al., 2005).

Differential Attentional Modulation of WS Neurons Phase Locked to Local Gamma

A closer look at the phase distributions revealed that WS neurons phase locked to gamma during successful allocation of attention (i.e., in correct trials) preferentially fired in either the trough or at the peak of the gamma cycle (Figure 4I). In addition to temporally sharpening WS responses (Cardin et al., 2009; Hasenstaub et al., 2005) and increasing synchronization, gamma-rhythmic inhibition by FS-PV neurons is implicated in gating of inputs and in gain control (Tiesinga et al., 2004, 2008), with the phase of gamma influencing the efficacy by which excitatory inputs drive local WS responses (Womelsdorf et al., 2014). Optogenetic experiments have shown that synaptic inputs arriving in the trough of gamma (i.e., when the level of inhibition is lowest) evoke enhanced responses of local WS neurons, while inputs arriving in the opposite phase evoke diminished responses (Cardin et al., 2009; Siegle et al., 2014). To directly investigate a potential relationship between endogenous gamma activity and responses of local mPFC WS neurons during attention, we selectively analyzed the firing rates during the delay of the WS neurons significantly phase locked to the trough or the peak of the gamma cycle in correct trials (Figures 5A and 5B). Interestingly, this separated the WS neurons into two sub-populations, with WS neurons discharging in the trough of gamma displaying increased firing and WS neurons discharging at the peak displaying suppressed firing (Figure 5C).

Top-Down Control of Attention Relies on FS-PV Activity

The strong network and behavioral correlate of mPFC FS-PV activities imply a functional role of this population in top-down control of attention and goal-directed behavior. In order to directly address this hypothesis, we employed optogenetic silencing of the FS-PV neurons during the delay. Light-activated inhibiting chloride-conducting channels were recently developed through structure-guided transformation of an originally cation-conducting channelrhodopsin (Berndt et al., 2014). Inhibitory channels hold several advantages over the traditionally used inhibitory pumps, including a more physiological inhibition of action potentials. SwiChR is a fast and bistable inhibitory step-function channel that can be used for inhibition of neuronal spiking for seconds (Berndt et al., 2014). Brief blue light application results in stable inhibition that can be terminated by application of red-shifted light. To confirm the bistable inhibitory action of SwiChR in vivo, we performed recordings in prelimbic/infralimbic cortex of PV-Cre mice injected with AAV DIO SwiChR-EYFP (n = 4 PV-Cre mice; Figure S5A). Blue light application (1 s, 473 nm, 5 mW) inhibited FS-PV spiking, resulting in disinhibition of neurons in the local circuit for several seconds, which could be counteracted by application of red light (1 s, 638 nm, 5 mW; Figures S5B–S5D). We expressed SwiChR bilaterally in mPFC PV neurons (Figures 6A and 6B) in trained animals (n = 5 PV-Cre mice) and pseudorandomly silenced the mPFC PV neurons' activity during the delay in 50% of the trials (total number of trials: 4,362). In separate sessions, 0.5, 1.0, or 2.0 s pulses of blue light (473 nm, 5 or 7 mW) were used (for experimental outline, see Figure S1A). Inhibition of FS-PV activity was terminated with 1 s of red light (638 nm; 5 mW) directly after the delay in all trials with SwiChR application. In essence,

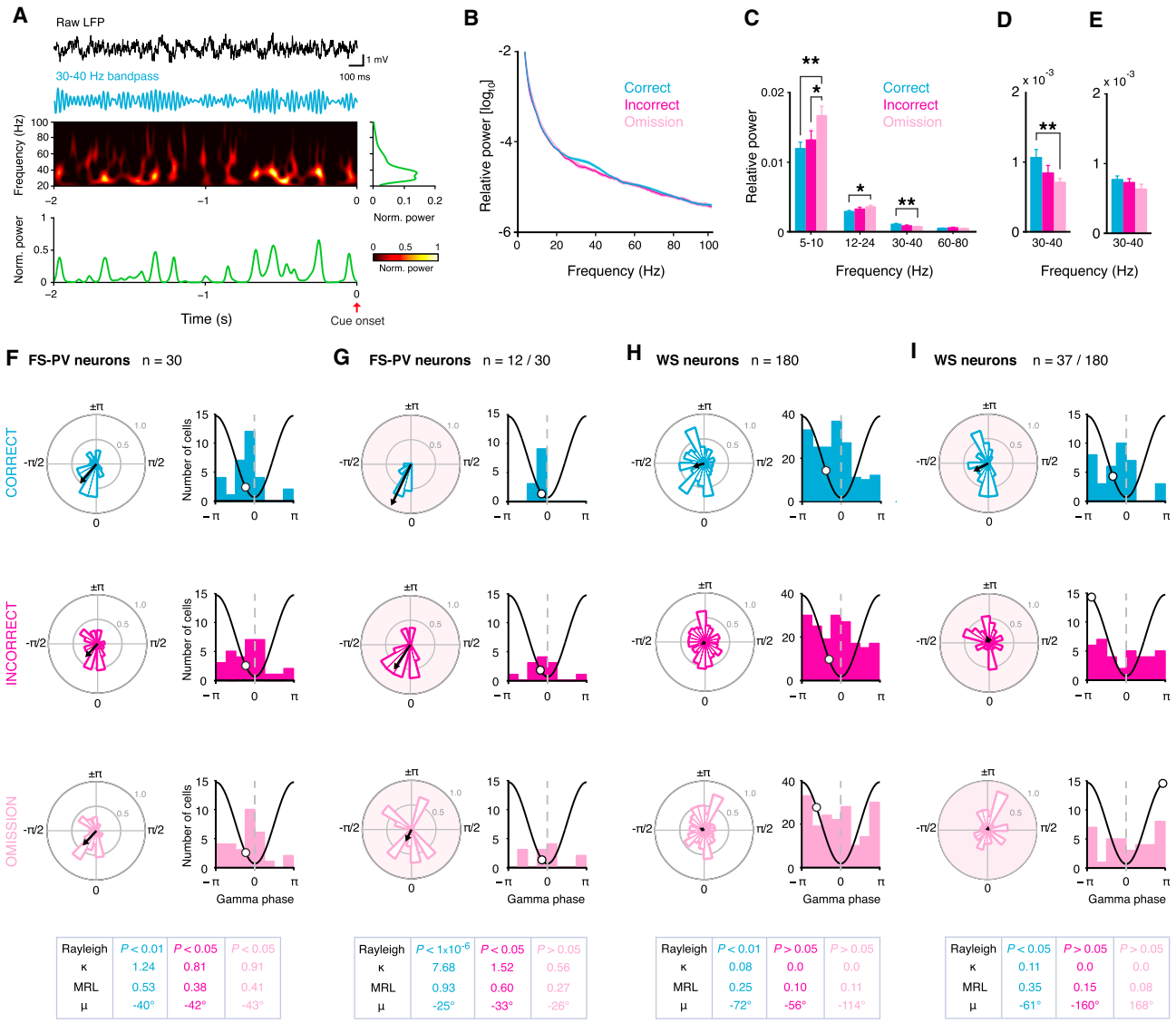

F	Rayleigh	$P < 0.01$	$P < 0.05$	$P < 0.05$
	κ	1.24	0.81	0.91
	MRL	0.53	0.38	0.41
	μ	-40°	-42°	-43°

G	Rayleigh	$P < 1x10^{-6}$	$P < 0.05$	$P > 0.05$
	κ	7.68	1.52	0.56
	MRL	0.93	0.60	0.27
	μ	-25°	-33°	-26°

H	Rayleigh	$P < 0.01$	$P > 0.05$	$P > 0.05$
	κ	0.08	0.0	0.0
	MRL	0.25	0.10	0.11
	μ	-72°	-56°	-114°

I	Rayleigh	$P < 0.05$	$P > 0.05$	$P > 0.05$
	κ	0.11	0.0	0.0
	MRL	0.35	0.15	0.08
	μ	-61°	-160°	168°

Figure 4. Successful Allocation of Attention Is Characterized by Synchronization of mPFC FS-PV and WS Neurons and Enhanced Gamma Oscillations

(A–D) and (F–I) Data from the last 2 s of the delay.

(A) Raw LFP, band-pass filtered LFP (30–40 Hz), and spectrogram (20–100 Hz) from a correct trial, including the average power (right green trace) and average 30–40 Hz band power (bottom green trace) of the spectrogram.

(B) Average relative LFP power (1–100 Hz) based on behavioral outcome. Shaded areas, SEM.

(C) Average relative LFP power in different frequency bands. The activity in the gamma band (30–40 Hz) is significantly elevated during successful allocation of attention (correct trials, blue) compared to trials with omission (pink); $p < 0.01$, paired t test. Error bars, mean ± SEM.

(D) Close-up of the 30–40 Hz activity in (C).

(E) 30–40 Hz activity directly after termination of the delay (i.e., during the cue; 0 to 1 s after cue onset). The level of gamma does not differ between trial types ($p > 0.1$, one-way ANOVA with repeated measures). Error bars, mean ± SEM.

(F–I) (Left) Circular distribution of the mean-spike gamma-phase angles (15° bin width) based on behavioral outcome. (Black arrow) Direction and magnitude (length) of the MRL for the population (MRL, 1.0 = exact phase synchronization of the neurons). (Right) Distribution of mean-spike gamma-phase angles (45° bin width) based on behavioral outcome. (Black line) One schematic gamma cycle. (White circle) Mean phase angle (μ). (Bottom) Table with population-phase-locking statistics. κ = circular concentration coefficient.

(F) Data for FS-PV neurons with ≥ 50 spikes during the last 2 s of the delay (n = 30; i.e., all FS-PV neurons).

(G) Data for FS-PV neurons with ≥ 50 spikes during the last 2 s of the delay and significant phase locking to gamma in correct trials ($p < 0.05$, Rayleigh test, n = 12 / 30). The firing of FS-PV neurons is most synchronized in correct trials (peak at 26.5 ± 1.7 ms, 30–40 Hz gamma).

(H) Data for WS neurons with ≥ 50 spikes during the last 2 s of the delay (n = 180).

(I) Data for WS neurons with ≥ 50 spikes during the last 2 s of the delay and significant phase locking to gamma in correct trials ($p < 0.05$, Rayleigh test, n = 37 / 180). This WS population becomes phase locked to gamma in correct trials (peak at 23.7 ± 5.2 ms, 30–40 Hz gamma).

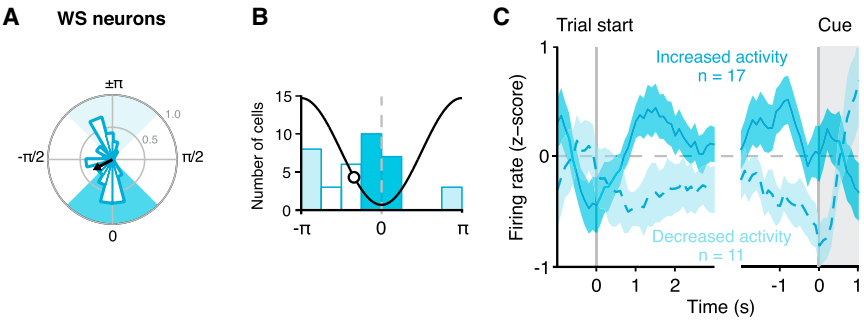

Figure 5. Gamma-Phase Modulation of WS Firing during Successful Allocation of Attention

(A–C) Data from correct trials, (A and B) same data as Figure 4I correct trials.

(A) Polar chart with color-coded gamma phases: blue, −45° to 45° refers to the trough of the gamma cycle; light blue, −135° to 135° refers to the peak of the gamma cycle. Circular distribution of the mean-spike gamma-phase angles (15° bin width) of the 37 WS neurons with ≥ 50 spikes during the last 2 s of the delay and significant phase locking to gamma in correct trials ($p < 0.05$, Rayleigh test).

(B) Distribution of mean-spike gamma-phase angles (45° bin width) for the neurons in (A). Colors as in (A).

(C) Firing modulation during the delay of the WS neurons in (B), firing in the trough (blue and solid line) or at the peak (light blue and dashed line) of the gamma cycle. Shaded areas, SEM.

we ensured that inhibition of FS-PV spiking matched the temporal pattern of elevated FS-PV activity during successful allocation of attention.

Inhibition of FS-PV neurons during attentional processing resulted in more than a doubling of the total number of errors (premature + incorrect + omission), regardless of blue light-pulse duration ($p < 0.01$, paired t test; Figure 6C). The major effect seen was a large increase in the number of omitted trials ($p < 0.01$, paired t test; Figures 6D and S6A). Omissions can reflect inattentiveness, particularly in mice, which are prone to withhold a response after failure to attend to the stimulus (Amitai and Markou, 2010). To investigate this further, we analyzed deficits in other domains. Analysis of the latency to collect reward after correct responses revealed that SwiChR silencing of mPFC FS-PV neurons did not affect reward latencies, independent of blue light-pulse duration and power intensity (Figures S6B and S6C), arguing against a general effect on internal motivation (Robbins, 2002).

Increased omissions could theoretically be attributed to deficits in motor activity (Robbins, 2002). Deficits in motor activity would be expected to be consistent in trials with SwiChR activation and, thus, independent of trial outcome, and we therefore analyzed the response latency (i.e., the reaction time) for correct responses. SwiChR application did not result in increased response latencies in correct trials with light application compared to correct trials without light, independent of blue-light-pulse duration and light intensity (Figures S6D and S6E). Together, these findings lend support to the notion that silencing of mPFC FS-PV activities during the delay selectively disrupts attentional processing.

Frequency-Dependent FS-PV Modulation of Attention

Optogenetic activation of cortical PV neurons has been employed in many studies investigating cortical computations (for review, see Hangya et al., 2014; Kepecs and Fishell, 2014; Roux et al., 2014). Optogenetic drive of FS-PV activity can, depending on the stimulation paradigm used and the network operations affected, lead to both perturbation (Sachidhanandam et al., 2013; Siegle et al., 2014) and enhancement (Lee et al., 2012; Siegle et al., 2014) of ongoing network activities and, ultimately, influence behavior (Pritchett et al., 2015). To directly investigate how synchronization of FS-PV firing at different frequencies influences attentional processing, we expressed ChR2 bilaterally in mPFC FS-PV neurons in a cohort of animals trained in the 3-CSRTT (n = 5 PV-Cre mice; Figures 7A and 7B). Blue light (473 nm, 3 ms light pulses, 5 or 7 mW) was applied throughout the pseudorandom delay (3, 4, or 5 s) or during the last 2 seconds of the delay pseudorandomly in 50% of the trials (total number of trials: 10,302; for experimental outline, see Figure S1A). Interestingly, optogenetic activation of FS-PV neurons at frequencies lower (1–10 Hz) than the native FS-PV activity displayed in correct trials directly before cue onset (19.25 ± 7.55 Hz, −1 to 0 s before cue onset) resulted in a significant increase in the total number of errors (premature + incorrect + omission; $p < 0.01$ paired t test; Figures 7C and S7A). As with the use of SwiChR, there was a large increase in the number of omitted trials ($p < 0.01$ paired t test; Figures 7D and S7B), but also the number of premature responses was increased with light application throughout the delay. Premature responses are thought to reflect deficits in impulse control, a PFC-dependent cognitive trait tightly linked to attentional processing. The negative effect on the behavior implies that intermittent forced synchronization of FS-PV neurons at low frequencies disrupts ongoing local network activities supporting attention. Our data further indicate that attention works in concert with response inhibition and that the two functions might share network underpinnings.

Activation at 20 Hz (i.e., close to the native FS-PV rate displayed before the cue in correct trials) did not change the error rate ($p > 0.1$, paired t test; Figures 7C, 7D, S7A, and S7B), indicating that synchronization of FS-PV activity per se does not disrupt attention. Despite extensive training, the animals do not correctly report the cue location in 100% of the trials. The most common error is an omission (Figures 6D and 7D), which presumably depends on a natural inability to sustain attention in every trial of a session. Improvement of behavior in the 3-CSRTT is thus possible, which is supported by pharmacological studies (Barak and Weiner, 2011). Optogenetic gamma drive of FS-PV neurons in barrel cortex was recently shown to enhance sensory perception (Siegle et al., 2014), and in line with this, we next activated the FS-PV neurons at gamma frequencies. Interestingly, activation of FS-PV neurons at 30–40 Hz during the delay resulted in a decreased rate of errors ($p = 0.01$, paired t test; Figure 7C), with a significant decrease in

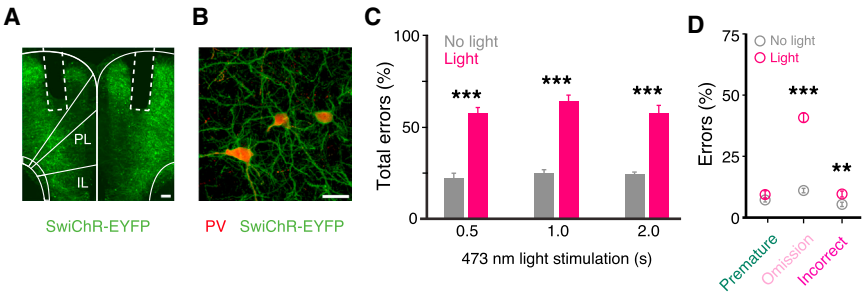

Figure 6. Silencing of mPFC FS-PV Neurons Disrupts Attentional Processing

(A) Placement of bilateral fiber optics and expression of SwiChR-EYFP (green) in mPFC FS-PV neurons in a PV-Cre mouse injected bilaterally with AAV DIO SwiChR-EYFP. 92.9% ± 2.4% of SwiChR-EYFP+ neurons expressed detectable levels of PV (742/802 neurons) and 83.9% ± 1.2% of PV+ neurons expressed SwiChR-EYFP close to the fiber tip (742/886 neurons). n = 5 PV-Cre mice. PL, prelimbic; IL, infralimbic.

(B) PV+ (red) mPFC neurons with SwiChR-EYFP expression (green) and typical PV interneuron morphology.

(C and D) Pseudorandom SwiChR application (red) during the delay in 50% of the trials. Activation: 0.5, 1.0, or 2.0 s of 473 nm in separate sessions; termination: 1 s 638 nm.

(C) Inhibition of mPFC FS-PV neurons during the delay results in more than a doubling of the total number of errors (premature + incorrect + omission) independent of blue light application (0.5, 1.0, or 2.0 s). Total errors: 59.8% ± 10.7% with light, 23.6% ± 6.4% without light; 0.5, 1.0, and 2.0 s combined.

(D) Inhibition of mPFC FS-PV neurons during the delay results in a large increase in the number of omitted trials. Data combined from 0.5, 1.0, and 2.0 s 473 nm light stimulation.

**p < 0.01, ***p < 0.001; error bars, mean ± SEM; Scale bars, (A) 100 μm; (B) 25 μm. See also Figures S5 and S6.

the number of omitted responses (p = 0.01 compared to trials without light, paired t test; Figure 7D), directly demonstrating that gamma synchronization of mPFC FS-PV neurons benefits attentional processing.

The pro-cognitive effects of gamma synchronization of FS-PV neurons were instant, short lasting, and specific to attention. Long-lasting effects are expected to be carried over to the pseudorandomly intermingled trials without light, but they were not (Figure 7C). The 30–40 Hz activation of FS-PV neurons did not affect motivation, as there was no significant difference in reward collection latencies between correct trials with or without light, regardless of the time point, power, or frequency of the light application (Figures S7C–S7E). As with the use of SwiChR, ChR2 application during the delay did not generate motor deficits, as the reaction time was not increased in correct trials with light compared to trials without light (Figures S7F–S7H).

DISCUSSION

Attention guides behavioral responses by selecting task-relevant information for further processing, and the signatures of attention have been extensively studied in sensory systems. Signals of attention arise in PFC (Baluch and Itti, 2011; Buschman and Miller, 2007; Li et al., 2010), a central site for executive control and coordination of goal-driven behavior. Studies in monkeys have consistently identified PFC as a key site for control of attention and a source of attentional modulation of neural responses in downstream brain structures (Clark et al., 2015; Gregoriou et al., 2014; Miller and Buschman, 2013; Moore and Armstrong, 2003; Rossi et al., 2007). However, the circuit underpinnings and mechanisms behind PFC's control of attentional processing have been largely unknown. More specifically, the computations by which PFC could communicate behavioral goals and contribute to selective enhancement of relevant representations in downstream areas have not been demonstrated. Further, a causal link between synchronous brain activity in attention and behavior has been missing (Gregoriou et al., 2015).

mPFC Neural Correlates of Attentional Processing in Goal-Directed Behavior

Our results firmly establish that mPFC FS-PV neurons are recruited by attentional processing and that enhanced and sustained FS-PV spiking predicts successful execution of goal-directed behavior. This surprisingly uniform modulation of mPFC FS-PV neurons constitutes a first cell-type-specific neural correlate of successful allocation of attention. We find that local WS neurons are separated into populations with suppressed or enhanced activity during attentional processing and that this separation is most pronounced during successful allocation of attention, possibly reflecting selective and optimal mPFC integration of the neuronal representations needed for achieving the goal. Our data do not reveal what representations are processed nor their cellular sources. The target and its value, the rules, and the goal of the task engage top-down attention (Clark et al., 2015) and are suggested representations needed to be actively maintained in mPFC during task performance.

The Role of Gamma in Attention

We find that successful allocation of attention is accompanied by elevated mPFC LFP activity in the gamma band and that elevated gamma is coupled to synchronous firing of FS-PV neurons and gamma-phase-dependent silencing of local WS neurons (Cardin et al., 2009). During enhanced gamma, local WS firing also became synchronized (Hasenstaub et al., 2005), supporting the view that gamma rhythm provides a means for formation of assemblies of WS neurons with coordinated firing (Buzsáki and Watson, 2012). Synchronization of pyramidal action potential firing is a proposed mechanism for how gamma rhythmicity could promote the relay of relevant information and drive firing in the proper targets with higher probability (Buzsáki and Watson, 2012; Salinas and Sejnowski, 2000, 2001). This could directly contribute to the preferential processing of task-relevant stimuli in downstream areas (Gregoriou et al., 2014) and, ultimately, to the behavioral benefits of attention.

Our data also suggest that the gamma rhythmic inhibition imposes phase-selective gain modulation of local WS neurons

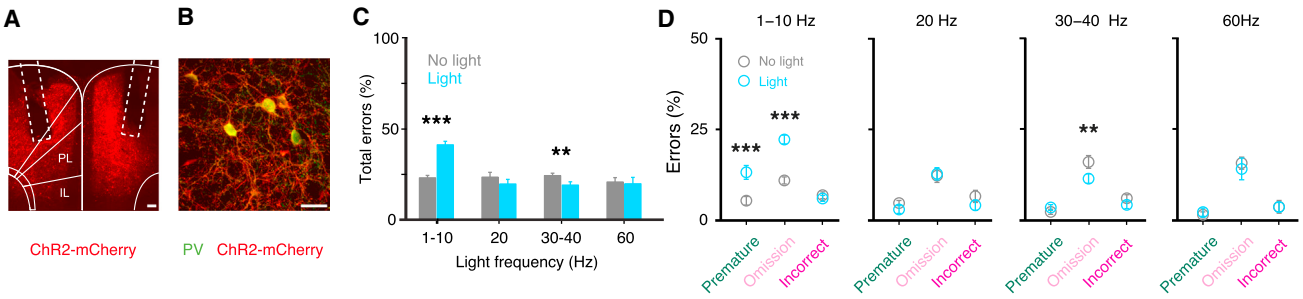

Figure 7. Frequency-Dependent FS-PV Modulation of Attentional Processing

(A) Placement of bilateral fiber optics and expression of ChR2-mCherry (red) in mPFC FS-PV neurons in a PV-Cre mouse injected bilaterally with AAV DIO ChR2-mCherry. 92,9% ± 1.0% of ChR2-mCherry+ neurons expressed PV (670/725 neurons) and 87.7% ± 0.8% of PV+ neurons expressed ChR2-mCherry close to the fiber tip (670/764 neurons); n = 5 PV-Cre mice; PL, prelimbic; IL, infralimbic.

(B) PV+ (green) mPFC neurons with ChR2-mCherry expression (red) and typical PV interneuron morphology.

(C and D) Pseudorandom ChR2 application (473 nm; blue) during the delay in 50% of the trials.

(C) Error rate with (blue) or without (gray) light application. The error rate in trials without light does not differ, regardless of stimulation frequency used in intermingled trials with light (1–10, 20, 30–40, or 60 Hz; $p > 0.1$ one-way ANOVA with repeated measures).

(D) Rate of different error types with (blue) or without (gray) light application. 30–40 Hz drive of FS-PV neurons reduces the number of omitted trials.

$^{**}p < 0.01$, $^{***}p < 0.001$; error bars, mean ± SEM. Scale bars, (A) 100 μm; (B) 25 μm. See also Figure S7.

during attention, which has been anticipated by modeling and optogenetic studies (Cardin et al., 2009; Pritchett et al., 2015; Siegle et al., 2014; Tiesinga et al., 2004, 2008). The cycles of strong FS-PV inhibition create brief time windows with decaying inhibition in the trough of gamma right before onset of the next gamma cycle, where WS neurons would be most sensitive to input and produce maximal output (Womelsdorf et al., 2014). Gamma rhythmic inhibition thus could enhance the throughput of task-relevant information both by synchronization of WS firing and by generating WS output with a higher spike probability. Taken together, our electrophysiological recordings support the view that the temporal conditions created by FS-PV firing specifically in the gamma range support computations underlying top-down control of attention and cognitive behavior (Fries, 2009).

The Role of mPFC PV-FS Neurons in Attention

Our SwiChR experiments show that silencing of mPFC FS-PV neurons during attentional processing has detrimental effects on goal-directed behavior. Based on our electrophysiological findings, it is conceivable that decreased inhibition by FS-PV neurons precludes proper gamma rhythmicity and prevents accurate synchronization and attentional modulation of local WS firing. As discussed, this is expected to impact the formation of WS assemblies and the relay to downstream structures.

While the finding of improved behavior with forced synchronization of mPFC FS-PV neurons at gamma frequencies can seem surprising, gamma oscillations have long been predicted to serve cognition (Gray and Singer, 1989), a concept recently finding direct experimental support. In optogenetic experiments, gamma drive of FS-PV neurons in PFC had pro-cognitive effects and could rescue deficits in cognitive flexibility (Cho et al., 2015). The pro-cognitive effects remained long term, which contrasts the instant and short-lasting effects in our study. Further, while Cho et al. (2015) used drive of gamma to rescue cognitive deficits in a mutant mouse, we demonstrate selective enhancement of attentional processing in overtrained normal mice. It thus appears that prefrontal gamma activity can support various aspects of cognitive processing on multiple timescales and probably through different circuit operations. It will be important for future studies to characterize the computations by which FS-PV gamma mediates particular constructs of cognition and under what contingencies.

The demonstration of frequency-dependent FS-PV modulation of attentional processing is conceptually important for our understanding of how synchronous brain activity can support cognition. This finding also agrees with the idea that oscillations are appropriate targets for investigation of pathophysiology of mental disorders characterized by changed cognition (Buzsáki and Watson, 2012) and, more specifically, that PV neurons play a key role in psychiatry (Hu et al., 2014). The pro-cognitive effects of synchronization of FS-PV neurons at gamma frequencies suggest that cell-type-specific manipulations can be used for enhancement of cortical computations and cognition. This concept is very encouraging, but it also underscores that, in order to understand the operations of the brain, we need to understand the component cells by their functions.

EXPERIMENTAL PROCEDURES

Mice were trained in the 3-CSRTT to attend to and report the location of a brief visual cue presented pseudorandomly in one of three cue/nose-poking holes (Figure S1A). To increase the attentional load, the cue was presented with pseudorandom delays (3, 4, or 5 s) after trial start. Nose-poking into the correct hole resulted in immediate access to reward, while incorrect reports, premature reports, and omitted responses were unrewarded and scored as errors, resulting in a 5 s timeout during which a new trial could not be initiated. Fully trained animals were implanted with microdrives holding tetrodes targeted to mPFC, and chronic recordings were performed over a large number of 3-CSRTT trials for characterization of the recruitment and firing modulation of mPFC neurons during attentional processing. Cell-type classification of local FS-PV and WS neurons was performed by electrophysiological characterizations, and the classification of FS-PV neurons was verified with opto-tagging using ChR2 in freely moving animals. The activity patterns of FS-PV and WS neurons, respectively, were aligned to trial start and cue presentation, and the correlation between

the firing modulation and attentional processing was investigated. To examine population activity, peri-event time histograms (PETHs) for each unit were normalized in *Z* score and averaged across different trials (correct, incorrect, and omission). For examination of how the activities of the FS-PV and WS populations were modulated by attention, we calculated the attentional modulation index (AMI) 1 s before cue onset. To identify inhibitory putative monosynaptic connections from FS-PV to WS cells, we calculated cross-correlations of spike trains for pairs of simultaneously recorded neurons across correct and error trials. To investigate changes in the power of the LFP during attention and presentation of the cue, respectively, the relative power for different frequency bands was calculated and compared between trial types. To investigate the relationship between single-unit activity and LFPs, we performed spike-LFP phase-locking analysis for correct, incorrect, and omitted trials. To determine the instantaneous phase angle of unit spikes relative to gamma oscillations, the phase vector of the filtered LFP was estimated, and the significance of spike-LFP phase locking was tested using circular statistics. The degree of phase locking was evaluated by the length of the mean resultant vector (MRL, range 0–1) and the concentration parameter (κ). Cohorts of fully trained animals were injected with adeno-associated viruses encoding ChR2 or SwiChR for optogenetic in vivo manipulation of FS-PV activity during attentional processing. Light (5 or 7 mW) was delivered pseudorandomly in 50% of the trials of each session. For SwiChR, 0.5, 1.0, or 2.0 s of blue 473 nm light was delivered at trial start and 1.0 s of red 638 nm light directly after termination of the delay. For ChR2, blue light was applied throughout the delay or during the last 2 s of the delay. The inhibitory action of SwiChR was confirmed with acute recordings with silicon probes in anesthetized animals. Statistical differences were determined by paired t tests and ANOVA with repeated measures (for the effects of optogenetic manipulations). More details are given in Supplemental Experimental Procedures.

SUPPLEMENTAL INFORMATION

Supplemental Information includes Supplemental Experimental Procedures, seven figures, and four movies and can be found with this article online at http://dx.doi.org/10.1016/j.cell.2015.11.038.

AUTHOR CONTRIBUTIONS

H.K. modified the 3-CSRTT task and equipment; trained, injected, and implanted the animals; planned and performed the electrophysiological and optogenetic experiments; analyzed and plotted the data; and critically reviewed the manuscript. S.Ä.R aided in training, electrophysiological, and optogenetic experiments and performed histological analysis. X.W. trained animals, and K.D. provided SwiChR, supervised its use, and reviewed the manuscript. M.C. conceived the project, designed the experiments, analyzed the data, wrote the manuscript, and prepared the figures.

ACKNOWLEDGMENTS

We thank H. Shin, C.I. Moore, and K. Meletis for invaluable scientific discussions and H. Yang for the graphical abstract. This work was supported by a European Research Council Starting Grant (337069, M.C.), the Knut and Alice Wallenbergs Foundation (Wallenberg Academy Fellow Grant KAW 2012.0208, M.C.), a Ragnar Söderberg Fellow in Medicine Grant (M.C.), the Swedish Brain Foundation (Hjärnfonden, M.C.), and NIH (K.D).

Received: July 7, 2015
Revised: September 9, 2015
Accepted: November 11, 2015
Published: January 14, 2016

REFERENCES

Amitai, N., and Markou, A. (2010). Disruption of performance in the five-choice serial reaction time task induced by administration of N-methyl-D-aspartate receptor antagonists: relevance to cognitive dysfunction in schizophrenia. Biol. Psychiatry *68*, 5–16.

Atallah, B.V., Bruns, W., Carandini, M., and Scanziani, M. (2012). Parvalbumin-expressing interneurons linearly transform cortical responses to visual stimuli. Neuron *73*, 159–170.

Baluch, F., and Itti, L. (2011). Mechanisms of top-down attention. Trends Neurosci. *34*, 210–224.

Barak, S., and Weiner, I. (2011). Putative cognitive enhancers in preclinical models related to schizophrenia: the search for an elusive target. Pharmacol. Biochem. Behav. *99*, 164–189.

Bari, A., Dalley, J.W., and Robbins, T.W. (2008). The application of the 5-choice serial reaction time task for the assessment of visual attentional processes and impulse control in rats. Nat. Protoc. *3*, 759–767.

Berndt, A., Lee, S.Y., Ramakrishnan, C., and Deisseroth, K. (2014). Structure-guided transformation of channelrhodopsin into a light-activated chloride channel. Science *344*, 420–424.

Buschman, T.J., and Miller, E.K. (2007). Top-down versus bottom-up control of attention in the prefrontal and posterior parietal cortices. Science *315*, 1860–1862.

Buzsáki, G., and Wang, X.J. (2012). Mechanisms of gamma oscillations. Annu. Rev. Neurosci. *35*, 203–225.

Buzsáki, G., and Watson, B.O. (2012). Brain rhythms and neural syntax: implications for efficient coding of cognitive content and neuropsychiatric disease. Dialogues Clin. Neurosci. *14*, 345–367.

Cardin, J.A., Carlén, M., Meletis, K., Knoblich, U., Zhang, F., Deisseroth, K., Tsai, L.H., and Moore, C.I. (2009). Driving fast-spiking cells induces gamma rhythm and controls sensory responses. Nature *459*, 663–667.

Carlén, M., Meletis, K., Siegle, J.H., Cardin, J.A., Futai, K., Vierling-Claassen, D., Rühlmann, C., Jones, S.R., Deisseroth, K., Sheng, M., et al. (2012). A critical role for NMDA receptors in parvalbumin interneurons for gamma rhythm induction and behavior. Mol. Psychiatry *17*, 537–548.

Cho, K.K., Hoch, R., Lee, A.T., Patel, T., Rubenstein, J.L., and Sohal, V.S. (2015). Gamma rhythms link prefrontal interneuron dysfunction with cognitive inflexibility in Dlx5/6(+/-) mice. Neuron *85*, 1332–1343.

Clark, K., Squire, R.F., Merrikhi, Y., and Noudoost, B. (2015). Visual attention: Linking prefrontal sources to neuronal and behavioral correlates. Prog. Neurobiol. *132*, 59–80.

Courtin, J., Chaudun, F., Rozeske, R.R., Karalis, N., Gonzalez-Campo, C., Wurtz, H., Abdi, A., Baufreton, J., Bienvenu, T.C., and Herry, C. (2014). Prefrontal parvalbumin interneurons shape neuronal activity to drive fear expression. Nature *505*, 92–96.

Donnelly, N.A., Paulsen, O., Robbins, T.W., and Dalley, J.W. (2015). Ramping single unit activity in the medial prefrontal cortex and ventral striatum reflects the onset of waiting but not imminent impulsive actions. Eur. J. Neurosci. *41*, 1524–1537.

Fries, P. (2009). Neuronal gamma-band synchronization as a fundamental process in cortical computation. Annu. Rev. Neurosci. *32*, 209–224.

Fujisawa, S., Amarasingham, A., Harrison, M.T., and Buzsáki, G. (2008). Behavior-dependent short-term assembly dynamics in the medial prefrontal cortex. Nat. Neurosci. *11*, 823–833.

Gold, J.M., Fuller, R.L., Robinson, B.M., Braun, E.L., and Luck, S.J. (2007). Impaired top-down control of visual search in schizophrenia. Schizophr. Res. *94*, 148–155.

Gray, C.M., and Singer, W. (1989). Stimulus-specific neuronal oscillations in orientation columns of cat visual cortex. Proc. Natl. Acad. Sci. USA *86*, 1698–1702.

Gregoriou, G.G., Gotts, S.J., Zhou, H., and Desimone, R. (2009). High-frequency, long-range coupling between prefrontal and visual cortex during attention. Science *324*, 1207–1210.

Gregoriou, G.G., Rossi, A.F., Ungerleider, L.G., and Desimone, R. (2014). Lesions of prefrontal cortex reduce attentional modulation of neuronal responses and synchrony in V4. Nat. Neurosci. *17*, 1003–1011.

Gregoriou, G.G., Paneri, S., and Sapountzis, P. (2015). Oscillatory synchrony as a mechanism of attentional processing. Brain Res. *1626*, 165–182.

Hangya, B., Pi, H.J., Kvitsiani, D., Ranade, S.P., and Kepecs, A. (2014). From circuit motifs to computations: mapping the behavioral repertoire of cortical interneurons. Curr. Opin. Neurobiol. *26*, 117–124.

Hasenstaub, A., Shu, Y., Haider, B., Kraushaar, U., Duque, A., and McCormick, D.A. (2005). Inhibitory postsynaptic potentials carry synchronized frequency information in active cortical networks. Neuron *47*, 423–435.

Hayden, B.Y., Smith, D.V., and Platt, M.L. (2009). Electrophysiological correlates of default-mode processing in macaque posterior cingulate cortex. Proc. Natl. Acad. Sci. USA *106*, 5948–5953.

Hu, H., Gan, J., and Jonas, P. (2014). Interneurons. Fast-spiking, parvalbumin^{+} GABAergic interneurons: from cellular design to microcircuit function. Science *345*, 1255263.

Isomura, Y., Harukuni, R., Takekawa, T., Aizawa, H., and Fukai, T. (2009). Microcircuitry coordination of cortical motor information in self-initiation of voluntary movements. Nat. Neurosci. *12*, 1586–1593.

Kepecs, A., and Fishell, G. (2014). Interneuron cell types are fit to function. Nature *505*, 318–326.

Korotkova, T., Fuchs, E.C., Ponomarenko, A., von Engelhardt, J., and Monyer, H. (2010). NMDA receptor ablation on parvalbumin-positive interneurons impairs hippocampal synchrony, spatial representations, and working memory. Neuron *68*, 557–569.

Kvitsiani, D., Ranade, S., Hangya, B., Taniguchi, H., Huang, J.Z., and Kepecs, A. (2013). Distinct behavioural and network correlates of two interneuron types in prefrontal cortex. Nature *498*, 363–366.

Lee, S.H., Kwan, A.C., Zhang, S., Phoumthipphavong, V., Flannery, J.G., Masmanidis, S.C., Taniguchi, H., Huang, Z.J., Zhang, F., Boyden, E.S., et al. (2012). Activation of specific interneurons improves V1 feature selectivity and visual perception. Nature *488*, 379–383.

Lewis, D.A., Curley, A.A., Glausier, J.R., and Volk, D.W. (2012). Cortical parvalbumin interneurons and cognitive dysfunction in schizophrenia. Trends Neurosci. *35*, 57–67.

Li, L., Gratton, C., Yao, D., and Knight, R.T. (2010). Role of frontal and parietal cortices in the control of bottom-up and top-down attention in humans. Brain Res. *1344*, 173–184.

Lustig, C., Kozak, R., Sarter, M., Young, J.W., and Robbins, T.W. (2013). CNTRICS final animal model task selection: control of attention. Neurosci. Biobehav. Rev. *37* (9 Pt B), 2099–2110.

Marín, O. (2012). Interneuron dysfunction in psychiatric disorders. Nat. Rev. Neurosci. *13*, 107–120.

Miller, E.K., and Buschman, T.J. (2013). Cortical circuits for the control of attention. Curr. Opin. Neurobiol. *23*, 216–222.

Moore, T., and Armstrong, K.M. (2003). Selective gating of visual signals by microstimulation of frontal cortex. Nature *421*, 370–373.

Noudoost, B., Chang, M.H., Steinmetz, N.A., and Moore, T. (2010). Top-down control of visual attention. Curr. Opin. Neurobiol. *20*, 183–190.

Pritchett, D.L., Siegle, J.H., Deister, C.A., and Moore, C.I. (2015). For things needing your attention: the role of neocortical gamma in sensory perception. Curr. Opin. Neurobiol. *31*, 254–263.

Robbins, T.W. (2002). The 5-choice serial reaction time task: behavioural pharmacology and functional neurochemistry. Psychopharmacology (Berl.) *163*, 362–380.

Rossi, A.F., Bichot, N.P., Desimone, R., and Ungerleider, L.G. (2007). Top down attentional deficits in macaques with lesions of lateral prefrontal cortex. J. Neurosci. *27*, 11306–11314.

Roux, L., and Buzsáki, G. (2015). Tasks for inhibitory interneurons in intact brain circuits. Neuropharmacology *88*, 10–23.

Roux, L., Stark, E., Sjulson, L., and Buzsáki, G. (2014). In vivo optogenetic identification and manipulation of GABAergic interneuron subtypes. Curr. Opin. Neurobiol. *26*, 88–95.

Sachidhanandam, S., Sreenivasan, V., Kyriakatos, A., Kremer, Y., and Petersen, C.C. (2013). Membrane potential correlates of sensory perception in mouse barrel cortex. Nat. Neurosci. *16*, 1671–1677.

Salinas, E., and Sejnowski, T.J. (2000). Impact of correlated synaptic input on output firing rate and variability in simple neuronal models. J. Neurosci. *20*, 6193–6209.

Salinas, E., and Sejnowski, T.J. (2001). Correlated neuronal activity and the flow of neural information. Nat. Rev. Neurosci. *2*, 539–550.

Siegle, J.H., Pritchett, D.L., and Moore, C.I. (2014). Gamma-range synchronization of fast-spiking interneurons can enhance detection of tactile stimuli. Nat. Neurosci. *17*, 1371–1379.

Sohal, V.S., Zhang, F., Yizhar, O., and Deisseroth, K. (2009). Parvalbumin neurons and gamma rhythms enhance cortical circuit performance. Nature *459*, 698–702.

Stark, E., Eichler, R., Roux, L., Fujisawa, S., Rotstein, H.G., and Buzsáki, G. (2013). Inhibition-induced theta resonance in cortical circuits. Neuron *80*, 1263–1276.

Tiesinga, P.H., Fellous, J.M., Salinas, E., José, J.V., and Sejnowski, T.J. (2004). Inhibitory synchrony as a mechanism for attentional gain modulation. J. Physiol. Paris *98*, 296–314.

Tiesinga, P., Fellous, J.M., and Sejnowski, T.J. (2008). Regulation of spike timing in visual cortical circuits. Nat. Rev. Neurosci. *9*, 97–107.

Totah, N.K., Kim, Y.B., Homayoun, H., and Moghaddam, B. (2009). Anterior cingulate neurons represent errors and preparatory attention within the same behavioral sequence. J. Neurosci. *29*, 6418–6426.

Totah, N.K., Jackson, M.E., and Moghaddam, B. (2013). Preparatory attention relies on dynamic interactions between prelimbic cortex and anterior cingulate cortex. Cereb. Cortex *23*, 729–738.

Vinck, M., Womelsdorf, T., Buffalo, E.A., Desimone, R., and Fries, P. (2013). Attentional modulation of cell-class-specific gamma-band synchronization in awake monkey area v4. Neuron *80*, 1077–1089.

Wilson, N.R., Runyan, C.A., Wang, F.L., and Sur, M. (2012). Division and subtraction by distinct cortical inhibitory networks in vivo. Nature *488*, 343–348.

Womelsdorf, T., Valiante, T.A., Sahin, N.T., Miller, K.J., and Tiesinga, P. (2014). Dynamic circuit motifs underlying rhythmic gain control, gating and integration. Nat. Neurosci. *17*, 1031–1039.

Zhang, S., Xu, M., Kamigaki, T., Hoang Do, J.P., Chang, W.C., Jenvay, S., Miyamichi, K., Luo, L., and Dan, Y. (2014). Selective attention. Long-range and local circuits for top-down modulation of visual cortex processing. Science *345*, 660–665.